Understanding the effect of water transport on the thermal expansion properties of the perovskites BaFe0.6Co0.3Nb0.1O3-δ and BaCo0.7Yb0.2Bi0.1O3-δ

Majewski, Artur; Slater, Peter; Steinberger-Wilckens, Robert

DOI:
10.1007/s10853-020-04994-9

License:
Other (please specify with Rights Statement)

Document Version
Peer reviewed version

Citation for published version (Harvard):
Majewski, A, Slater, P & Steinberger-Wilckens, R 2020, 'Understanding the effect of water transport on the thermal expansion properties of the perovskites BaFe0.6Co0.3Nb0.1O3-δ and BaCo0.7Yb0.2Bi0.1O3-δ', *Journal of Materials Science*, vol. 55, no. 28, JMSC-D-20-02913R2, pp. 13590-13604. https://doi.org/10.1007/s10853-020-04994-9

Journal of Materials Science

Understanding the effect of water transport on the thermal expansion properties of the perovskites BaFe0.6Co0.3Nb0.1O3-δ and BaCo0.7Yb0.2Bi0.1O3-δ

--Manuscript Draft--

Manuscript Number:	JMSC-D-20-02913R2
Full Title:	Understanding the effect of water transport on the thermal expansion properties of the perovskites BaFe0.6Co0.3Nb0.1O3-δ and BaCo0.7Yb0.2Bi0.1O3-δ
Article Type:	Manuscript (Regular Article)
Keywords:	negative thermal expansion; perovskite; solid oxide cell; water incorporation
Corresponding Author:	Artur Jacek Majewski University of Birmingham Birmingham, UNITED KINGDOM
Corresponding Author Secondary Information:	
Corresponding Author's Institution:	University of Birmingham
Corresponding Author's Secondary Institution:	
First Author:	Artur Jacek Majewski
First Author Secondary Information:	
Order of Authors:	Artur Jacek Majewski
	Peter Raymond Slater, Professor
	Robert Steinberger-Wilckens, Professor
Order of Authors Secondary Information:	
Abstract:	In this paper, we report a study of the perovskite phases, BaFe0.6Co0.3Nb0.1O3-δ (BFCN) and BaCo0.7Yb0.2Bi0.1O3-δ (BCYB), as possible air electrode materials for solid oxide cells (SOCs). The crystal structures and thermal and chemical expansion properties are reported, and the stability evaluated in different atmospheres. The thermal expansion data show unusual behaviour, with apparent negative thermal expansion (NTE) behaviour at low temperatures (100-240oC) up to -11.6x10−6 K−1 for BFCN and up to -17.3x10−6 K−1 for BCYB. This NTE behaviour is related to water incorporation at lower temperatures, which is then lost in this temperature range upon heating. In order to examine the potential of these materials for use in a solid oxide electrolyser (SOE), the stability at elevated temperatures in the presence of water was evaluated, which indicated that water vapour leads to increased degradation at SOC operation temperatures.
Funding Information:	Engineering and Physical Sciences Research Council (EP/R023662/1) — Professor Peter Raymond Slater

Understanding the effect of water transport on the thermal expansion properties of the perovskites $BaFe_{0.6}Co_{0.3}Nb_{0.1}O_{3-\delta}$ and $BaCo_{0.7}Yb_{0.2}Bi_{0.1}O_{3-\delta}$

Artur Jacek Majewski[1]*, Peter Raymond Slater[2], Robert Steinberger-Wilckens[1]

[1] School of Chemical Engineering, University of Birmingham, Birmingham, B15 2TT, UK

[2] School of Chemistry, University of Birmingham, Birmingham, B15 2TT, UK

* a.j.majewski@bham.ac.uk

Abstract

In this paper, we report a study of the perovskite phases, $BaFe_{0.6}Co_{0.3}Nb_{0.1}O_{3-\delta}$ (BFCN) and $BaCo_{0.7}Yb_{0.2}Bi_{0.1}O_{3-\delta}$ (BCYB), as possible air electrode materials for solid oxide cells (SOCs). The crystal structures and thermal and chemical expansion properties are reported, and the stability evaluated in different atmospheres. The thermal expansion data show unusual behaviour, with apparent negative thermal expansion (NTE) behaviour at low temperatures (100-240°C) up to -11.6x10^{-6} K^{-1} for BFCN and up to -17.3x10^{-6} K^{-1} for BCYB. This NTE behaviour is related to water incorporation at lower temperatures, which is then lost in this temperature range upon heating. In order to examine the potential of these materials for use in a solid oxide electrolyser (SOE), the stability at elevated temperatures in the presence of water was evaluated, which indicated that water vapour leads to increased degradation at SOC operation temperatures.

Keywords: negative thermal expansion, perovskite, solid oxide cell, water incorporation

1. Introduction

Solid oxide cells (SOCs) are attracting considerable interest due to their high efficiency in energy conversion as both solid oxide fuel cells (SOFC) and solid oxide electrolysers (SOE). However, there are still many problems related to the chemical stability and reliability of the components, due to the high operating temperatures of 650 to 950°C. It is a known fact that the performance of the air electrode is one of the most important factors that limits SOC performance. Therefore, a lot of research in recent years has concentrated on the development and optimisation of air electrode materials for SOCs [1-3]. The SOC air electrode must exhibit high electronic and ionic conductivity, mechanical and chemical stability in the temperature range 500 to 950°C and at the oxygen partial pressure of 1x10^{-5} to 1 atmosphere. Widely studied air electrodes can be divided into two groups: materials which are predominantly electronic conductors like $La_{1-x}Sr_xMnO_{3-\delta}$ (LSM) [4] with poor ionic transport properties, and a group of mixed oxygen and electronic conductors (MIEC) such as $Ba_{0.5}Sr_{0.5}Co_{0.8}Fe_{0.2}O_{3-\delta}$ (BSCF) [5-7] or $La_{0.6}Sr_{0.4}Co_{0.2}Fe_{0.8}O_{3-\delta}$ (LSCF) [8,9]. The mixed-conducting class of materials also includes a subclass of Triple Conducting Oxides (TCO) [10,11] that exhibits high levels of conductivity of three charge carriers: oxygen ions, protons, and electron holes (or electrons). The triple

($e^-/O^{2-}/H^+$) conducting oxides are relatively rare due to the challenge related to H^+/e^- recombination issues [12]. Existing electrodes used in SOE and SOFC that represent TCO behaviour are typically composites made of proton conductors mixed with electron-oxygen conductors [12-15]. Protonic ceramic fuel cells allow the potential to obtain exceptional power densities and long term stability at a low temperature of 500^{o}C [14]. Therefore, all reports that can relate the water incorporation characteristics to the crystal structure of MIEC are of high value.

For SOC materials, the match in the thermal expansion coefficient (TEC), αL, of components is a very important factor that determines their practical application. Mismatch in TEC leads to interfacial mechanical stress and may consequently result in delamination or crack formation. Usually, cell materials are therefore selected according to the TEC of the chosen electrolyte. The most common 8YSZ electrolyte has a thermal expansion coefficient of 10.5×10^{-6} K^{-1}, leading to an expansion of 10.5 nm of a sample of 1 mm length during heating by 1 K [16]. The mismatch between the TEC of an electrolyte and the respective electrodes should be as low as possible and must be less than 50% of the electrolyte thermal expansion to prevent any negative mechanical effects [17].

Most materials expand on heating and shrink upon cooling (under constant pressure). The asymmetry of interatomic potential results in a positive coefficient of thermal expansion (PTE). However, contraction upon heating can be observed for some materials [18]. For solid materials, many physical or physicochemical processes can cause the phenomenon of negative thermal expansion (NTE) with an increase in temperature. The most frequently reported ones are phase transitions (ice/water), electronic valence transitions [19-21], ferroelectric ordering [22-24], contraction of zeolites (siliceous or ZrW_2O_8) by changing in bridging M-O-M bond angles [25-27], or orbital and magnetic ordering [28]. While there have been some reports of perovskite materials with NTE during the last three decades [29-33], such observations are unusual as perovskites in the form ABO_3 generally do not exhibit NTE properties [30]. Another factor that is important for thermal expansion characteristics, particularly for perovskite systems in SOC operation, are the changes to the composition. For example, it is a well-known fact that the formation of an oxygen vacancy in perovskites results in the expansion of their lattice because of the reduction in the transition metals (TM) oxidation state. As an example, such chemical expansion is responsible for around 20-30% of the overall thermochemical expansion for the LSCF electrode heated in the air [17]. The shrinkage behaviour of SOC materials has also been observed and is attributed to a chemical process, with the oxidation of Ni to NiO [34] as a typical illustration. In terms of overall SOC operation, it is therefore important, that materials can expand/contract thermally and chemically simultaneously to avoid stress build-up. Therefore, in the analysis of expansion data, distinguishing between processes is important, with the presence of chemical expansion resulting in non-linearity in the overall lattice expansion. Indeed, for proton-conducting ceramics, the TEC can be affected by chemical expansion related to the hydration reaction that results in an increase in the crystal lattice size due to water incorporation [35]. Oxygen vacancies act as sites for proton incorporation in a humid atmosphere with the following processes possible due to either water or oxygen incorporation:

$$H_2O + V_O^{\bullet\bullet} + O_O^x \leftrightarrow 2OH_O^{\bullet} \quad (1)$$

$$H_2O + 2h^{\bullet} + 2O_O^x \leftrightarrow 2OH_O^{\bullet} + \frac{1}{2}O_2(g) \quad (2)$$

$$\frac{1}{2}O_2(g) + V_O^{\bullet\bullet} \leftrightarrow O_O^x + 2h^{\bullet} \quad (3)$$

where $V_O^{\bullet\bullet}$ is an oxygen vacancy, O_O^x an oxygen site in the host lattice, $OH_O^{\bullet}$ a hydroxyl group in the hydrated structure (a proton attached to lattice oxygen), and $h^{\bullet}$ represents an electron hole (corresponds to oxidation of the transition metal). For proton-conducting electrolytes, the hydration is the only chemical expansion process since the metal oxidation states are typically independent of p_{O_2}[36]. Muñoz-García and Pavone [12] reported that changes to the cell size of proton-conducting perovskites can be explained by the formation of OH-O hydrogen bonds that distort the average perovskite structure and modify the TM-O-TM bond angles when hydrated. It was reported [37] that for proton-conducting electrodes in reducing conditions, the hydration process should be conducted at the operating temperature to reduce stress related to the resultant cell expansion. The changes in lattice size due to the chemical process of dehydration depend on the dopant concentration which affects the level of oxygen vacancies available for water incorporation [38].

Most reported studies on perovskite candidates for SOC devices have dealt with the impact of temperature on thermal expansion. Studies that consider the effect of moisture in the synthesis and in the testing process are rare. As reported by many authors [39,35,40,13,15,17,41], water is incorporated into oxygen vacancy sites in perovskite systems. Despite recent progress, the understanding of the interaction of the transition metal-containing perovskite electrodes with moisture, and their phase stability (at SOC conditions) is lacking. This is especially important with the increase in the application of proton-conducting SOCs, where the moisture content at the air electrode can be much higher than 4% [42]. Therefore, developing new SOC air electrode materials and understanding the proton incorporation behaviour is of key scientific and technical importance.

$BaFe_{0.6}Co_{0.3}Nb_{0.1}O_{3-\delta}$ (BFCN) and $BaCo_{0.7}Yb_{0.2}Bi_{0.1}O_{3-\delta}$ (BCYB) are interesting candidates for SOC. $BaFe_{1-x-y}Co_xNb_yO_{3-\delta}$ (BFCN) was reported to have an electric conductivity around 15 S cm^{-1} but the very high oxygen transport properties with D_{chem} value of 4.51×10^{-5} cm^2 s^{-1} at 650°C makes it a very interesting candidate for a SOC electrode [43]. BFCN requires Nb doping above y=0.08 for pure cubic structure, while below that value it shows mixed cubic/hexagonal structure [44]. Higher Fe content in BFCN was reported to improve the stability, however, electrical conductivity and oxygen permeability are lower [45]. Also deficiency at the A-side $Ba_{0.9}$ of BFCN was reported to improve stability [46]. BCYB is a much less known material, with the trivalent Yb element added for the creation of oxygen vacancies and the possibility for mediating water incorporation and hence generating the protonic conductivity similar to proton-conducting electrolytes.

In this work, we investigate the thermal expansion behaviour and stability of the perovskite systems $BaFe_{0.6}Co_{0.3}Nb_{0.1}O_{3-\delta}$ (BFCN) and $BaCo_{0.7}Yb_{0.2}Bi_{0.1}O_{3-\delta}$ (BCYB). Both structures are cubic perovskites as synthesised. In our exploratory study of the **$BaFe_{0.9-x}Co_xNb_{0.1}O_{3-\delta}$** solid solution, x=0.3 was the highest Co

composition for which preliminary results indicated a cubic cell. For **$BaCo_{0.7}Yb_{0.2}Bi_{0.1}O_{3-\delta}$,** exploratory studies showed that through Yb and Bi co-doping, a cubic perovskite could be obtained without Fe. Both selected materials show evidence for the incorporation of water and that makes them potential candidates for proton-conducting cells. Dilatometry and XRD studies showed negative TEC at low temperatures. The observed negative TEC was shown to be associated with temperature-induced desorption of water, which is discussed in this paper.

2. Experimental

2.1. Materials synthesis

Samples of $BaFe_{0.6}Co_{0.3}Nb_{0.1}O_{3-\delta}$ (BFCN) and $BaCo_{0.7}Yb_{0.2}Bi_{0.1}O_{3-\delta}$ (BCYB) were prepared via the conventional solid-state reaction method. Analytical-grade powders $BaCO_3$, Fe_2O_3, Co_3O_4, Nb_2O_5, Yb_2O_3 and Bi_2O_3, (commercially available) were initially mixed with a mortar and pestle, according to the molar ratios of Ba:Fe:Co:Nb = 1:0.6:0.3:0.1 and Ba:Co:Yb:Bi = 1:0.7:0.2:0.1. The obtained mixtures were heated first at 950°C, ground and heated at 1,050°C (BFCN) and 1,100°C (BCYB) for 12 h in ambient air. Sintered samples were then crushed, ground and sieved through sieve 100 nm and used for analyses and pellets preparation.

To prepare cylindrical pellets (8 mm diameter), samples of the synthesised powders (0.5 g) were cold-isostatic pressed at 10k psi. All pellets were sintered in air at 1,100°C, for 4 h at a heating rate of 5°C min^{-1}. The density of the sintered pellets was 4 determined by gas pycnometer micrometrics AccuPyc II.

2.2. Characterisation

The two obtained $BaFe_{0.6}Co_{0.3}Nb_{0.1}O_{3-\delta}$ and $BaCo_{0.7}Yb_{0.2}Bi_{0.1}O_{3-\delta}$ materials were characterised using standard measurement techniques. The linear thermal expansion of pelletised materials was assessed using a Netzsch DIL402C dilatometer according to ASTM E228−17 [47] with alumina as the reference material in the dry air flow of 50 ml min^{-1} in the range 25 to 1,000°C, at a heating rate of 5°C min^{-1}. Temperature-dependent mass change profiles (TGA) in dry air (pO_2=0.21 atm, 50 ml min^{-1}) were obtained using a Netzsch 209F1 instrument, evaluated between room temperature and 1,000°C, at a heating rate of 5°C min^{-1}, corrected for the instrumental error. Samples (10 to 20 mg) of the sintered perovskites were also examined by temperature-programmed oxidation (TPO). TGA and differential scanning calorimeter DTA analyses in N_2 (50 ml min^{-1}) were conducted using a Netzsch STA 449 instrument coupled to a mass spectrometer Netzsch QMS 403. Hydration of the air electrode powders was analysed by isothermal TGA measurements using the Netzsch 209F1. Samples were dehydrated at 900°C in dry air:N_2 1:1 mixture (N_2 as protective gas), the temperature was lowered to 300°C and after reaching equilibrium (around 130 min) humid air:N_2 (pH_2O=0.02 atm) was connected.

The crystal structure of the samples was determined by powder x-ray diffraction (XRD). XRD patterns (room temperature and high temperature) were collected with a D8 ADVANCE (Bruker) diffractometer with Cu Ka radiation. XRD patterns were collected in the temperature range 25 to 900°C (heating rate 5°C min^{-1}), with 1

h temperature stabilisation at each measured step. The structural refinements of the XRD scans (the lattice parameters and phase fractions) were analysed with GSAS-II software based on the Rietveld method [48]. Analysis of the microstructure and chemical elemental composition were conducted using an SEM Hitachi TM3030Plus equipped with EDS. High-resolution TEM scans were obtained using an FEI Talos 200X Scanning/Transmission microscope (S/TEM) with EDS. TEM scans were analysed using GATAN software. All analysed samples were in the sintered at 1100°C powder form.

3. Results and discussion

3.1. Phase analysis

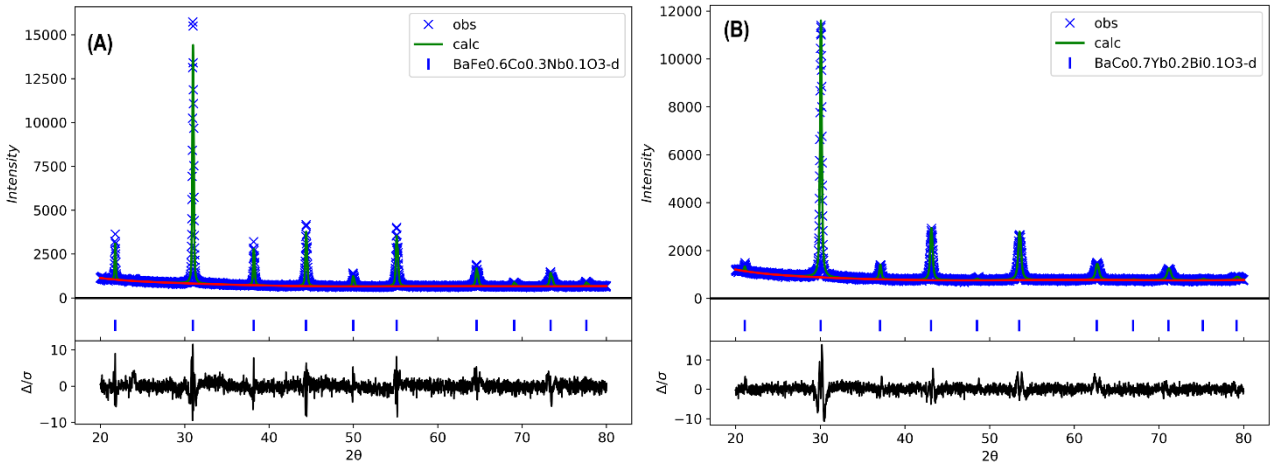

Fig.1. Observed, calculated and difference XRD patterns for (A) $BaFe_{0.6}Co_{0.3}Nb_{0.1}O_{3-\delta}$ and (B) $BaCo_{0.7}Yb_{0.2}Bi_{0.1}O_{3-\delta}$ at 25°C.

Fig.1 shows the XRD patterns and the results of Rietveld refinements for the synthesised BFCN and BCYB powders (at 25°C). All the diffraction peaks could be indexed to a cubic structure with space group Pm-3m (Fig.1) according to the refinement by software GSAS-II. For BFCN the cell length was a=b=c= 4.07667(12)Å, with cell volume V= 67.751(6)$Å^3$, and the goodness-of-fit (GOF) was 1.49. For BCYB the cell length was a=b=c= 4.1845(5) Å, cell volume V= 73.272(26)$Å^3$, the GOF was 1.57. The lattice parameters of these new perovskite systems are not available in literature, but for the similar structure of $BaCo_{1-x-y}Fe_xNb_yO_{3-\delta}$ (x=0.2-0.8, y=0.2-0.5), the lattice constants of the cubic phases were reported from 4.05 to 4.06 Å [49], which is similar to the results obtained here for BFCN. The theoretical density of BFCN was 6.032 and for BCYB 6.480 g cm^{-3}, as calculated from of Rietveld refinements of XRD scans.

3.2. Microstructure - TEM

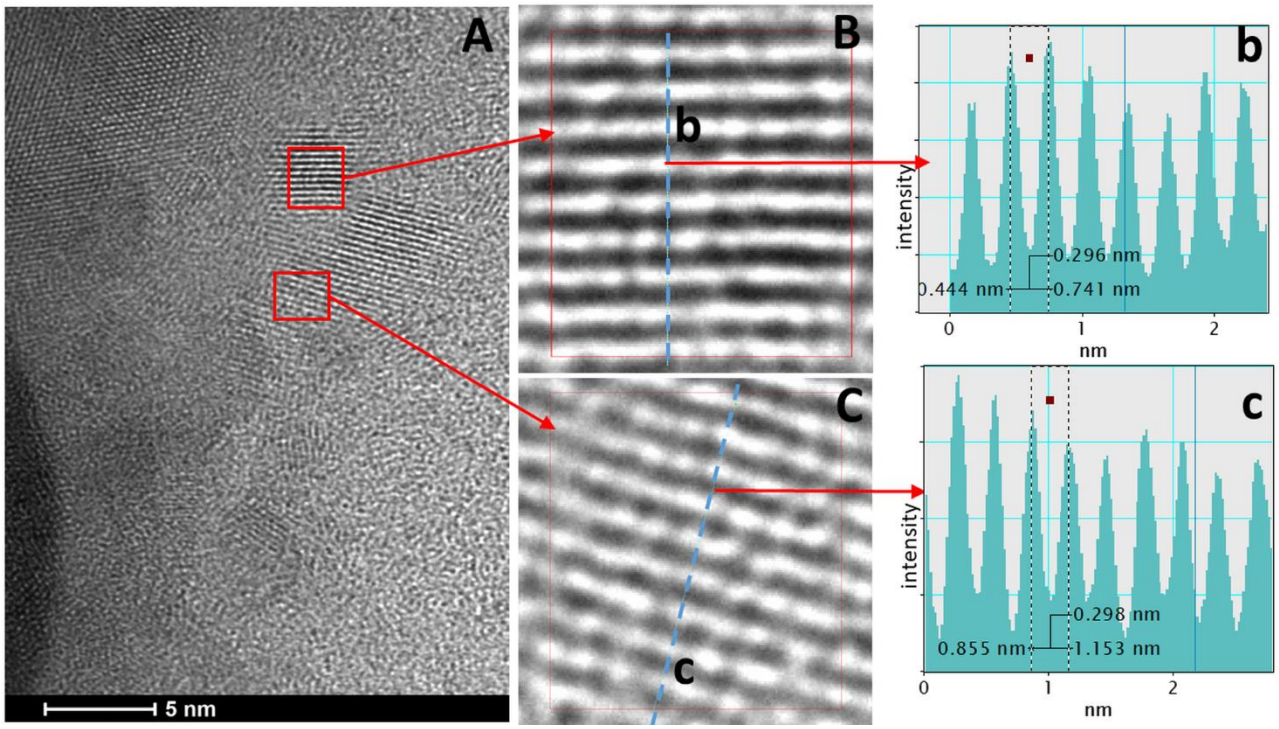

Fig.2. HR-TEM images of the structure of $BaFe_{0.6}Co_{0.3}Nb_{0.1}O_{3-\delta}$ (A) and magnified areas (B) and (C); (b) and (c) show the normalised intensity across lattice profiles.

The morphology and size of particles were analysed by SEM (Fig.9A and C - discussed later) and TEM (Fig.2 and 3). Fig.2A shows the TEM results for BFCN. The crystallites were spherical, with an average size of 5 to 10 nm. The analysis of TEM scans for BFCN revealed the existence of well-ordered structures composed of grains with a uniform spacing (Fig.2B and C). Fig. 2b and c show the nominal intensity of the lattice cross-section perpendicular to the planes for two different grains. The distance between planes around 0.3 nm corresponded to the d-spacing between [110] planes of the structure $d=a\sqrt{2}$. These TEM data confirm that BFCN has a uniform crystal structure.

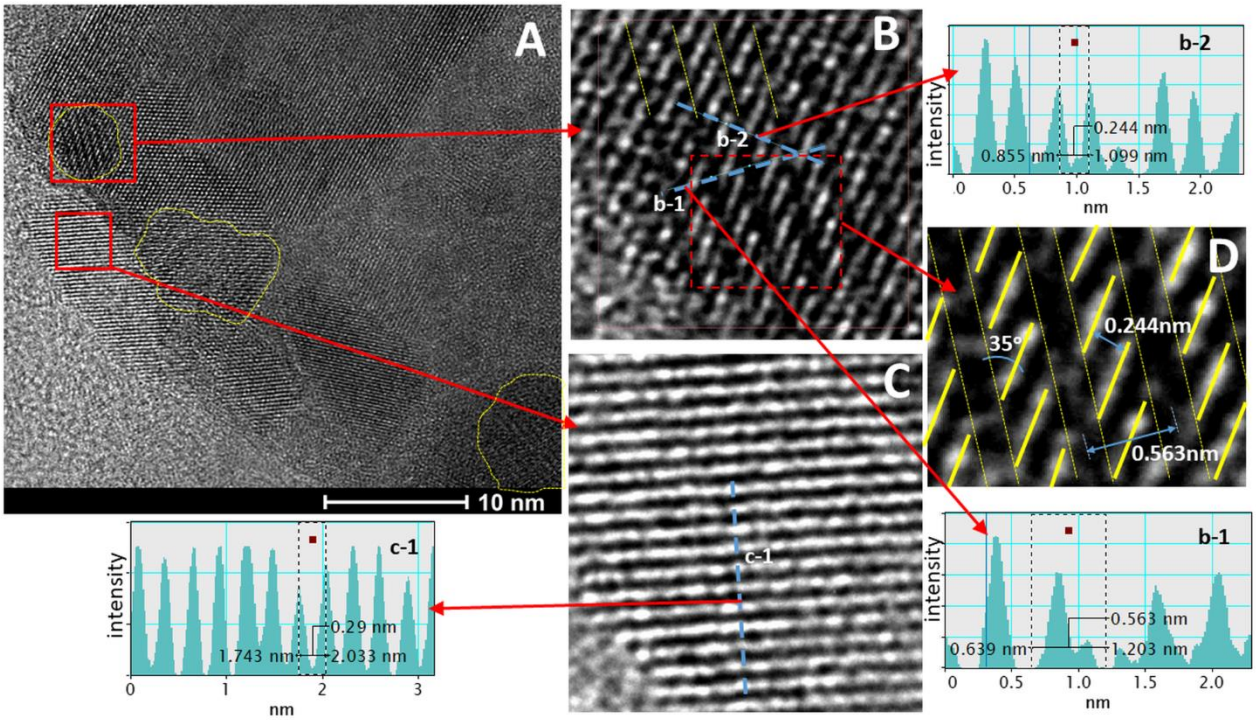

Fig.3. HR-TEM images of the structure of $BaCo_{0.7}Yb_{0.2}Bi_{0.1}O_{3-\delta}$. (A) and the magnified areas: (C) the dominant lattice structure; (B) and (D) the 2D-type lattice structure (marked with the yellow dashed line in part A); (b1), (b-2) and (c-1) show the normalised intensity across the lattice profiles.

In contrast to $BaFe_{0.6}Co_{0.3}Nb_{0.1}O_{3-\delta}$ (BFCN), the TEM data for the perovskite $BaCo_{0.7}Yb_{0.2}Bi_{0.1}O_{3-\delta}$ (BCYB) was more complex showing some interesting differences, which may be due to the presence on the B-site of cations with significantly different ionic radii. High-resolution TEM scans for BCYB revealed an added complexity and the formation of two distinct features. What was believed to be a single-phase structure (at room temperature, XRD-Fig.1B) appeared to be a mixture of two phases. The TEM analyses were executed at multiple areas of the sample, with a sample result presented in Fig.3A. A vertically aligned phase was visibly embedded in the dominant bulk phase as presented in Figs.3A and B. However, EDS scans did not reveal any significant changes in sample composition in the different regions. Fig.3b-1, b-2 and c-1 present the nominal intensity of the planes in cross-sections perpendicular to lattice structures. The dominating bulk lattice structure had a distance between layers of around 0.3 nm (Fig.3C-c1), which could represent the d-spacing between [110] planes of the structure as for BCYB. The nature of the second phase is unclear at the moment. XRD at room temperature suggested a single-phase perovskite, however, at elevated temperature; the presence of two perovskite phases was detected (see XRD results at elevated temperature Fig.6b and 7c-d). Future studies are required to clarify this complex nature.

3.3. Effect of temperature on thermal expansion and mass change

Thermal expansion characteristics of the sintered BFCN and BCYB materials were evaluated using dilatometry and high-temperature XRD. Figs.4 A and B display the linear thermal expansion $\Delta L/L$ (black curves) and TGA

analyses (red curves) of the BFCN and BCYB samples (samples were analysed in the temperature range 25 to 1,000°C in dry air). The pellets used for the dilatometry measurement had density 80-90%.

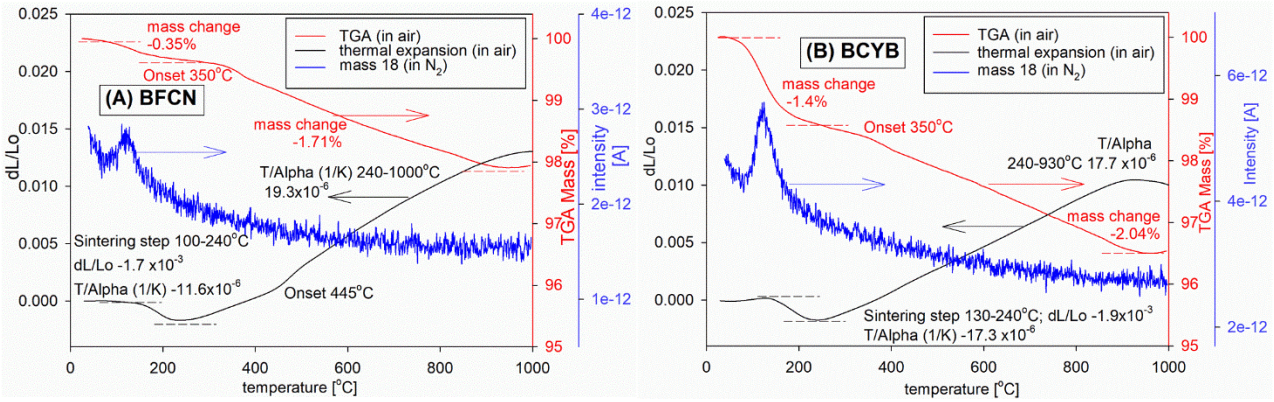

Fig.4. Linear thermal expansion ΔL/L and mass change (TGA) data for (A) $BaFe_{0.6}Co_{0.3}Nb_{0.1}O_{3-\delta}$ and (B) $BaCo_{0.7}Yb_{0.2}Bi_{0.1}O_{3-\delta}$ (25 to 1,000°C in dry air). Water evolution, as detected by the mass spectrometer, is represented by the blue curves (test in N_2 50 ml min^{-1}).

Fig.4A and B show evidence for a weight loss, with mass spectrometry results (mass 18) showing that this is due to loss of water. The water was incorporated into the structure after exposing sintered samples to humid air (pO2=0.20, pH_2O=0.04 atm) at room temperature for a minimum 24 h. The thermal expansion behaviour (dilatometry) of sintered BFCN and BCYB samples showed that this water loss resulted in sample contraction. The TGA mass change profiles (Fig.4) present a similar weight loss of around 2% observed for both BFCN and BCYB samples under dry air pO_2=0.21 atm. The rapid weight loss that occurred at temperatures below 200°C can thus be related to desorption of water. The BCYB sample showed a higher mass loss associated with water release, indicating greater water content for this phase; the mass change was -1.4% compared to -0.35% for BFCN. At higher temperatures (onset temperature around 350°C for both samples) further mass loss was observed, which can be attributed to oxygen loss and thus a reduction in Fe/Co oxidation state, as observed for other Fe/Co based perovskite electrode materials [50,51]. Only oxygen and water were detected by mass spectrometer with increase in temperature (test in N_2).

For similar samples of $BaFe_{1-x-y}Co_xNb_yO_{3-\delta}$ (BFCN), but with much higher Co content, NTE was not observed [43,46]. The reason for different expansion properties could be the higher Fe content and the related higher lattice parameter for the presented in this work BFCN. Waidha et al. [52] analysed water incorporation to $BaFe_{1-x}Co_xO_{3-\delta}$ structures and observed that the amount of water the sample can incorporate (and at the same time the possibilities of related negative thermal expansion upon heating and water release) strongly depends on the Fe:Co proportion. It was reported that the basicity of the oxide ions is another key parameter for water incorporation [15].

As highlighted above, the thermal expansion results (Fig.4) showed evidence for apparent NTE in a small temperature range attributed to chemical contraction due to water loss. The NTE was observed above 100°C

for BCFN and above 130°C for BCYB. The observed temperature range for this process was 140°C for BFCN and 110°C for BCYB. For BFCN the observed linear NTE αL was -11.6×10^{-6} K^{-1} (100 to 240°C) and the largest negative slope for the linear TEC corresponded to αL of -20.7×10^{-6} K^{-1} (150 to 210°C). For BCYB the NTE αL was -17.3×10^{-6} K^{-1} (130 to 240°C) and the largest negative slope for TEC corresponded to αL of -24.0×10^{-6} K^{-1} (150 to 210°C). For both samples, the shrinkage step concluded at 240°C and above this temperature, the TEC changed to positive, with $\alpha L=19.3\times10^{-6}$ K^{-1} for BCFN and $\alpha L=17.7\times10^{-6}$ K^{-1} for BCYB. The high overall TEC in this range can be attributed to the significant Co content at the B site, 30% for BFCN and 70% for BCYB. It has been shown previously that high Co concentration increases the TEC but improves the catalytic activity for exchange reactions on the electrode surface [53]. This can be in part explained [54] by the fact that Co has a tendency to change from low to high spin at elevated temperature resulting in an additional increase in ionic radii and consequently higher TEC. The higher TEC for BFCN is probably due to the high (90% of B site) transition metal content.

The change to the linearity in thermal expansion at a temperature above 450°C (Fig.4) can be attributed to the contribution of chemical expansion due to the reduction of transition metals (change to ionic radii) that is associated with oxygen loss and the oxygen vacancy formation. The tested materials BFCN and BCYB contained transition metals Fe/Co and Co respectively, which adopt a lower oxidation state on oxygen loss that has a larger ionic size and then results in the cell volume expansion of the cubic phase. The influence of changes in oxygen nonstoichiometry on lattice expansion was confirmed by the observed mass reduction (TGA measurements presented in Fig.4). The observed nonlinearity in TEC at a temperature above 900°C could be due to a drop in the contribution of chemical expansion to the overall thermal expansion, with most available Fe and Co already reduced and/or converted to higher spin.

To confirm that the observed NTE range was related to water loss from the structure, TGA measurements were performed in N_2 (with the evolving gas analysed by a mass spectrometer). A clear peak for the mass 18 (corresponding to water) data was observed at the detected NTE region. This peak was observed for both samples. The observed NTE and the fact that the desorption of water occurred at a temperature higher than 100°C indicated that the water was incorporated into the structure. The slow release of water upon heating (Fig.4A-B), with the peak observed at 150°C and the end of the process at around 600°C, suggests a strong interaction with the crystal structure.

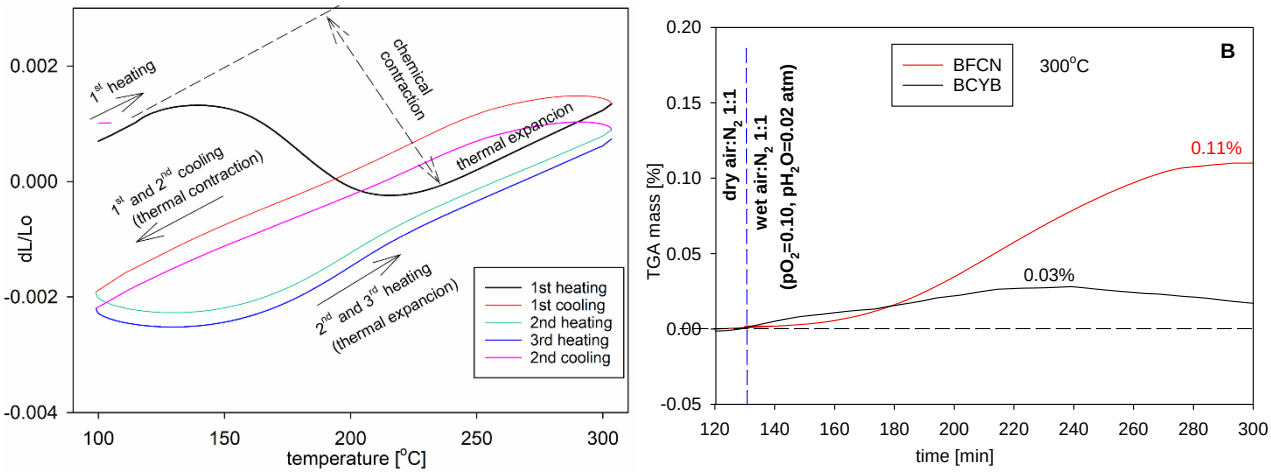

Fig.5. A) Linear thermal expansion $\Delta L/L$ for $BaFe_{0.6}Co_{0.3}Nb_{0.1}O_{3-\delta}$ 100-300°C in dry air upon temperature change. B) Mass changes for BFCN 128 mg and BCYB 102 mg of powders after the isothermal switch at 300°C from dry air:N_2 mixture to humid air:N_2 pH_2O=0.02, pO_2=0.10 atm.

The observed desorption of water at the temperature where the NTE was observed (Fig.5) prompted further investigation of the samples. Samples of BFCN and BCYB were heated to 300°C and cooled down to 100°C. The cycle was repeated three times in the dilatometer in a loop (Fig.5). Fast cooling of the chamber was achieved by circulating water through an external chiller. The NTE was observed only during the first-time heating for both BFCN and BCYB in dry conditions. After the first heating step, the sample behaved as a standard PTE material. This confirms that the initial presence of moisture in the samples gives rise to the apparent NTE. Interestingly, if a sample was left overnight at room temperature and ambient air conditions (around 4% H_2O), water incorporation occurred again and the NTE behaviour returned, thus showing that these perovskite systems show a tendency to incorporate water at low temperatures suggesting the reversible process of water incorporation and release.

Both materials (powders) were heated to 900°C and cooled to 300°C with 130 min stabilisation to dehydrate. After isothermal switching to humid air condition (air:N_2 1:1, pH_2O=0.02, pO_2=0.10 atm) both BFCN and BCYB showed weigh increase by exposure to water vapour at 300°C in air. BFCN mass increased by 0,11% and BCYB by 0.03% when switched from dry to the humid atmosphere (Fig5B). The gain is attributed to the incorporation of water (hydration) that depends on defect structure. Overall, the results confirmed that both materials can incorporate water and the desorption of water was responsible for the observed NTE of BFCN and BCYB. Thus, changes to the TEC of BFCN and BCYB can be driven by dehydration and hydration phenomena affected by changes in environmental humidity.

3.4. High-temperature XRD analysis

The samples were also analysed by high-temperature XRD to investigate in more detail the thermal expansion/contraction properties of the BFCN and BCYB structure. It is known that the TEC measured for bulk materials and calculated from the crystal lattice size change are correlated and often similar, but not

always interchangeable [17]. The high-temperature XRD scans were taken between 25 and 900°C to analyse the thermo-dehydration effects (Fig.6-7). To highlight the TEC behaviour, Fig.7A-D shows the evolution of prominent XRD peaks (peaks (110) and (200)) upon heating. All the remaining XRD peaks followed the same trend. All the diffraction peaks for both samples shifted to higher angles on heating, from 25 to 200°C for BFCN, and to 300°C for BCYB. This indicates lattice contraction and hence NTE for both compositions. Structure refinement based on the Rietveld method was performed using the XRD data to obtain detailed information about cell parameter changes. Fig.6 shows the dependence of unit cell edge, *a,* upon heating for BFCN and BCYB. The range where NTE occurred (ΔT) is highlighted by the shaded area and was analogous to that obtained from dilatometry.

The high-temperature XRD data for BCYB suggested that above room temperature, two similar perovskite phases were present, consistent with the observations of extra features in the TEM data. While at room temperature, the data could be fitted to a single cubic perovskite phase. At a higher temperature, a low angle shoulder was observed on all peaks indicating a second cubic perovskite phase with slightly larger unit cell size (these shoulders are indicated by "◊" Fig.7C-D). Therefore, for this BCYB sample, two-cubic perovskite phases were adopted for the refinement model, which gave a good fit to the data. The refinement results, showing the cell size, and phase fraction between the bulk core phase A and the minor phase B that appeared at elevated temperature, are presented in Fig.6B. The data show that both phases are present in the temperature range of 100 to 600°C, but above this temperature, the peaks merge again, and a single main phase is observed above 600°C. Phase A, with a smaller unit cell, was the dominant component in the whole temperature range studied, with the highest proportion of the larger cell size B phase (up to 40%) in the temperature range of 300 to 400°C. Interestingly, only the main phase A showed NTE (shrinkage of the cell size in the temperature range 150 to 350°C). Phase B showed a general expansion on heating. Above 300°C, both phases A and B showed an expansion in the unit cell size. The relative shrinkage step (phase A and B) $\Delta a/a0$ calculated from the refined lattice constants was -3.3×10^{-3} (25-300°C) which is close to $\Delta L/L0$ -1.9×10^{-3} (100-240°C) obtained from the dilatometer method. Since the XRD test was conducted under atmospheric conditions with some humidity present, this could explain the small difference in the thermal expansion behaviour and the small differences observed in the NTE zones relative to the dilatometer data.

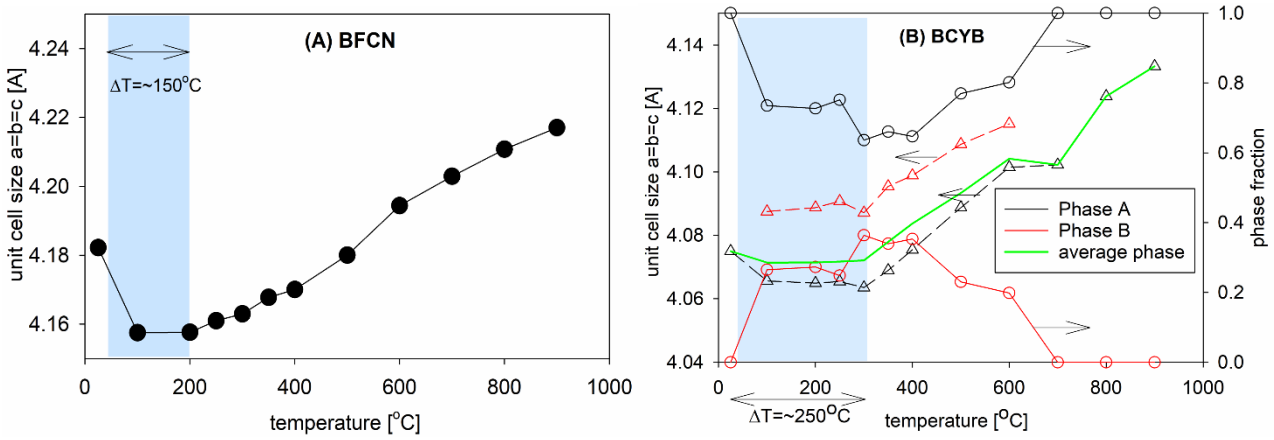

Fig.6. Change in lattice constants with temperature for (A) $BaFe_{0.6}Co_{0.3}Nb_{0.1}O_{3-\delta}$ and (B) $BaCo_{0.7}Yb_{0.2}Bi_{0.1}O_{3-\delta}$.

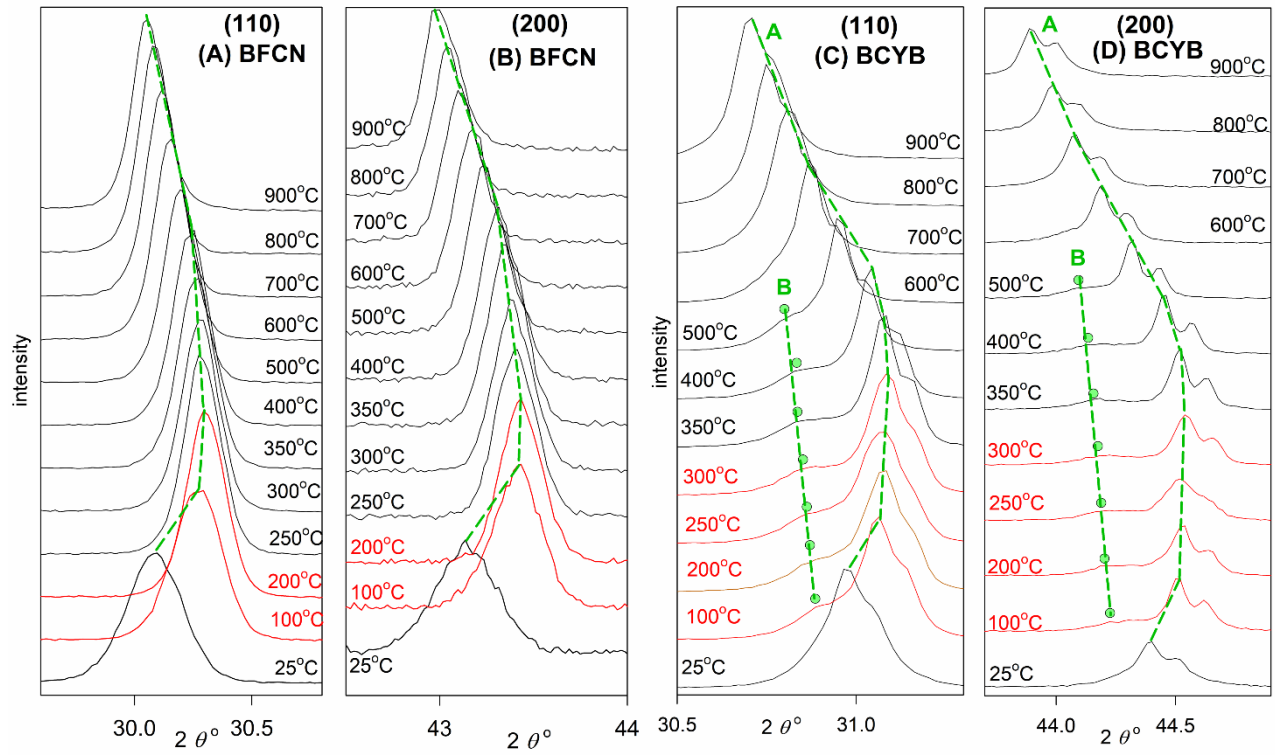

Fig.7. Temperature-dependent XRD patterns; prominent peaks (110) and (200) for $BaFe_{0.6}Co_{0.3}Nb_{0.1}O_{3-\delta}$ and $BaCo_{0.7}Yb_{0.2}Bi_{0.1}O_{3-\delta}$. Dashed green lines trace the shift of the peaks' maximum with temperature. The NTE range is highlighted in red.

In contrast to BCYB, BFCN remained cubic without peak splitting over the full temperature range, which confirms that the initial NTE and subsequent PTE was isotropic. In the low-temperature region, the cell volume was shown to decrease over a relatively broad temperature interval (ΔT of 175K), which was the same range where the water release was observed from TGA. The shrinkage step Δa/a0 calculated from the refined lattice constants was -24.6×10^{-3} (25-200°C). Above 250°C, PTE behaviour was observed, with a sharp increase in the unit cell size, which coincided with the results from the dilatometry data shown in Fig.4A.

3.5. Investigation into the effect of exposure to increased humidity

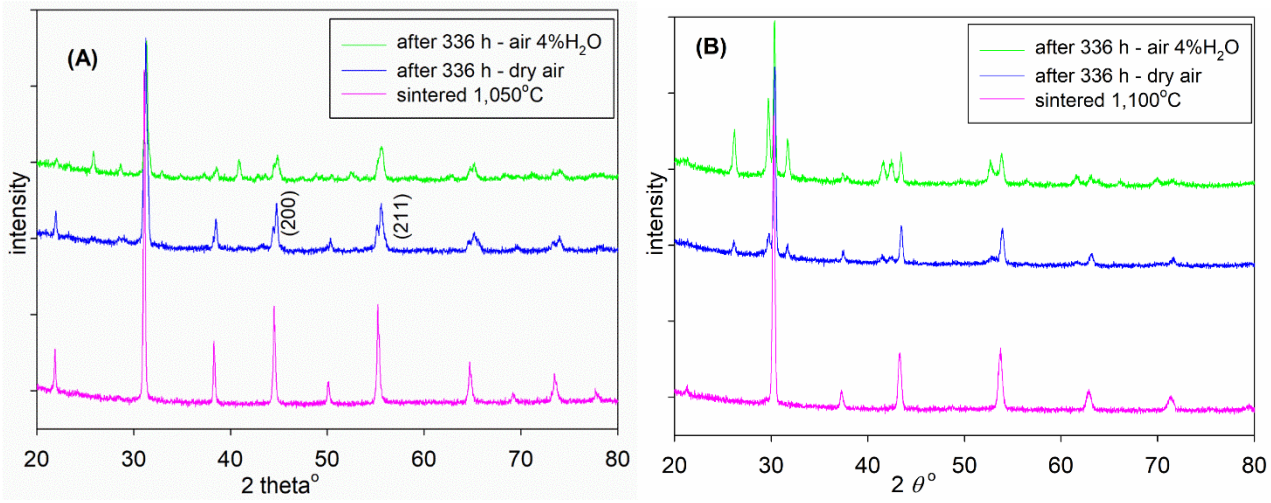

Fig.8. XRD scans for (A) $BaFe_{0.6}Co_{0.3}Nb_{0.1}O_{3-\delta}$ and (B) $BaCo_{0.7}Yb_{0.2}Bi_{0.1}O_{3-\delta}$, at 25°C, a fresh sample and exposed to dry and wet (pO_2=0.20, pH_2O=0.04 atm) air (100 ml min^{-1}) for 336 h at 750°C.

For mixed conducting oxides, the stability of phases under SOC operating conditions is a big concern for practical application as electrodes. To verify the phase stability, samples of BFCN and BCYB (1 g powder) were heated at an elevated temperature of 750°C in dry (pO_2=0.21) and wet (pO_2=0.20, pH_2O=0.04 atm) air (with pCO_2 around 0.0004 atm). Since any degradation could take a long time to occur, the samples were heated for a prolonged time of 336 h and then examined by XRD. After exposure to dry air (Fig.8 blue lines), the peaks broadened and some split, such as the (200) and (211) reflections for the BFCN sample (Fig.8A). The degradation behaviour in dry air showed the formation of a second cubic phase, rather than the generation of new crystalline structures, especially for BFCN (Fig.8.A). These changes could be related to instabilities in the perovskite phases due to their high tolerance values (the Goldschmidt tolerance factor for BFCN and BCYB was above unity, with 1.07 and 1.06 respectively), as observed for $Ba_{0.5}Sr_{0.5}Co_{0.8}Fe_{0.2}O_{3-\delta}$ (BSCF) heated under similar conditions [48]. Heat treatment under wet conditions led to greater degradation for both samples, with evidence of significant impurity phases ($BaCoO_{3-\delta}$, and unknown phases) (Fig.8 green line). Thus, the results suggest that the decomposition was catalysed by water at elevated temperatures.

As a result, it can be concluded that both samples BFCN and BCYB are unstable in SOC conditions and are most likely not suitable for practical applications.

3.6. Microstructure - SEM scans

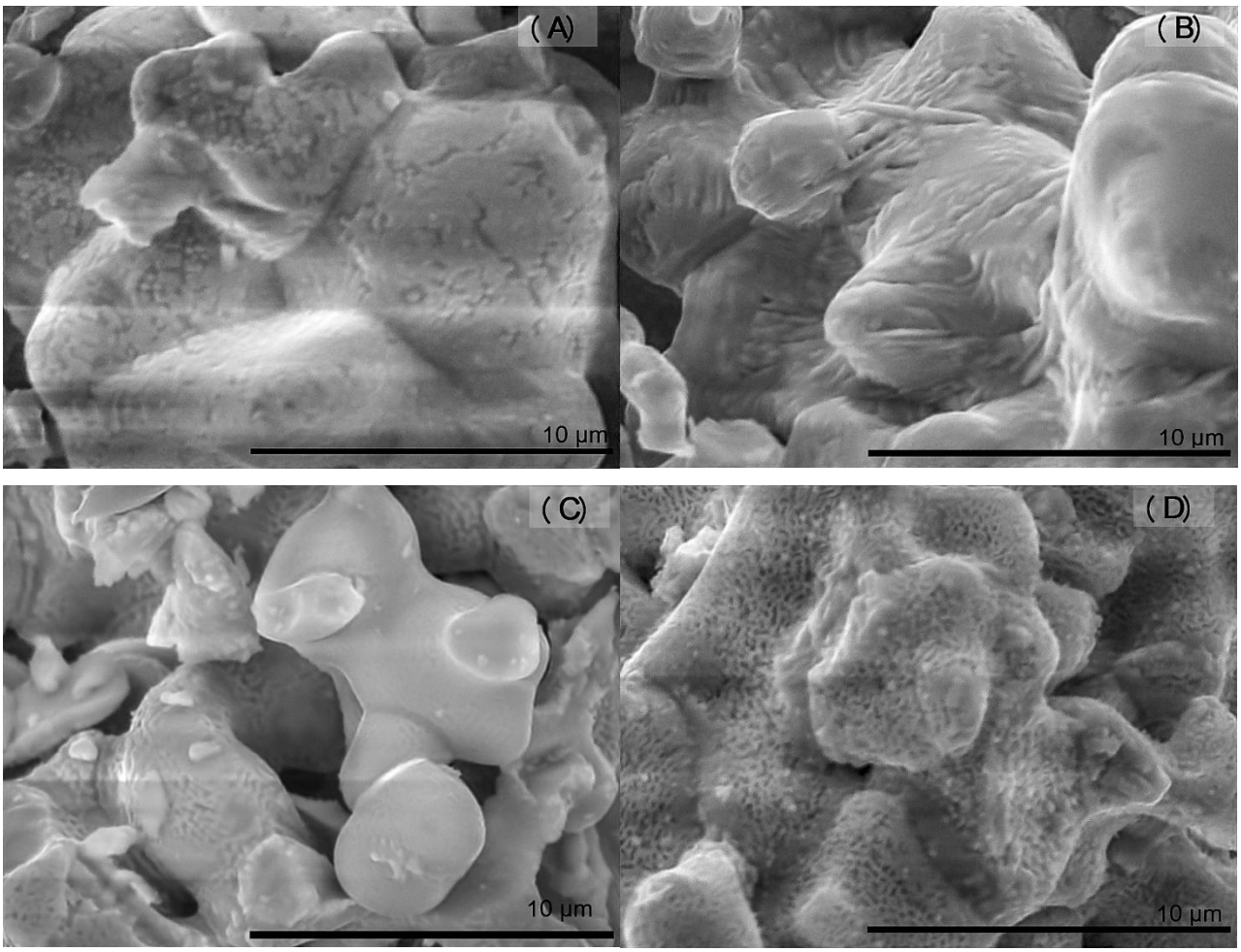

Fig.9. SEM scans of fresh sintered samples: (A) $BaFe_{0.6}Co_{0.3}Nb_{0.1}O_{3-\delta}$ and (C) $BaCo_{0.7}Yb_{0.2}Bi_{0.1}O_{3-\delta}$; and samples after exposure to humid air (pO_2=0.20, pH_2O=0.04 atm) at 750°C for 336 h: (B) $BaFe_{0.6}Co_{0.3}Nb_{0.1}O_{3-\delta}$ and (D) $BaCo_{0.7}Yb_{0.2}Bi_{0.1}O_{3-\delta}$.

Fig.9A and C present the SEM scans of BFCN and BCYB (respectively) samples. The microstructure was porous, composed of granular particles with an average size of 2 to 10 µm. The particle size estimated from the SEM scans was larger than the size estimated from TEM, which suggests that the grains were composed of several crystallites.

EDS analyses did not reveal significant changes in elemental composition. Comparing the SEM images before (Fig.9A and C) and after (Fig.9B and D) the exposure test, it is evident that the structure of both samples changed after exposure to humid conditions at high temperature (pO_2=0.20, pH_2O=0.04 atm air, 750°C). The surface of BCYB became rougher, and some particle sintering was also observed. The surface of the BFCN sample showed the formation of the features (Fig.9B), which suggests an expulsion of some particles. However, EDS scans did not indicate any significant change in composition.

4. Discussion

The perovskites BFCN and BCYB were examined as potential air electrodes for SOC. However, they were both unstable under SOC operating conditions, which indicates that they are not suitable as electrode candidates. From the results, several hours of exposure to humid air at high temperature was enough to start the degradation process of these perovskites. Previous reports [55,49] showing the decomposition of Ba containing perovskite systems under air electrode conditions have suggested that CO_2 in addition to water is responsible for the degradation. However, there was no evidence for the formation of $BaCO_3$ in the current samples.

Studying the stability of such materials towards humidity is important as the materials employed as an SOC air electrode system are exposed to air with up to 4% humidity. Moreover, in a proton-conducting SOC system, the water concentration will be much higher than 4%, since the water feed occurs at the air electrode. The water incorporation properties of perovskite systems and the mobility of these protons are essential for the electrochemical performance of air electrodes working in proton-conducting SOFCs However, most research on thermal expansion of SOC electrodes in literature concentrates on SOFC or SOE operation. Therefore, information about proton-conducting electrodes is rare. Therefore, the results presented here, showing water incorporation at low temperatures in these BFCN and BCYB systems, are significant, highlighting that if related systems with improved moisture stability can be prepared, they may be promising air electrode materials. Furthermore, the illustration that this subsequent water loss on heating leads to apparent NTE can help with understanding features in TEC studies and the further development of proton-conducting materials. The amount of water that can be incorporated depends on the concentration of oxygen vacancies. However, the proton content is usually small, and so the expansion effect is negligible for conventional air electrode materials. Therefore, the observed significant expansion/contraction due to hydration/dehydration in the systems studied here is significant in helping to direct future work in this area. Transition metal containing perovskites with NTE related to thermo-dehydration behaviour have to date not been studied in detail.

The detailed examination of the thermal expansion characteristics is also significant, since, in the SOC related literature, the change in cell size with temperature is usually reported as “thermal expansion“ without distinguishing between classic thermal expansion and the participation of chemical expansion. Our results for BFCN and BCYB show that several phenomena overlap, leading to interesting variations in TEC from NTE to PTE behaviour. Overall, the obtained TEC data upon heating showed the representative behaviour of: typical thermal expansion (due to the inherent vibrational properties), chemical shrinkage (due to dehydration), chemical expansion (due to the reduction of transition metal oxidation state) and chemical contraction (due to the removal of oxide ion and oxygen vacancy formation – the smaller size of $V_O^{\bullet\bullet}$ compared to O^{2-} [17]). The two contraction processes compete with the two expansion processes during the heating. Additionally, the dehydration increases the oxygen vacancy concentration (1), and the concentration of holes can also be affected (2). For the current samples, the majority of the dehydration reaction (1-3) occurred in the low-temperature range of 100 to 240°C in the tested dry conditions. In humid conditions, the

temperature of such changes was increased and could be as high as 700°C [41]. The volume contraction from dehydration (replacing $OH_O^{\bullet}$ defects with $V_O^{\bullet\bullet}$) and associated transition metal reduction overshadowed the thermal expansion resulting in apparent NTE - under dry air conditions. The observed decrease in the dimension due to water release has led some authors [56,57] to label this behaviour "pseudo-negative thermal expansion".

While the BFCN and BCYB samples have the potential to become TCOs due to the oxygen nonstoichiometry and the observed behaviour of water incorporation (hydration), there is a need to further improve the moisture tolerance at a higher temperature for the tested samples to consider them for practical application. Therefore, if the BCFN and BCTB stability can be improved, they can be considered as interesting candidates for SOCs and particularly for proton-conducting cells, considering their ability to incorporate water. While the water uptake potential for BFCN and BCYB was proven, the mobility of these protons needs to be investigated to determine the potential as TOC electrode. Our plans include investigating whether the co-substitution or increase in sintering temperature (as reported by Geng, Z., et al. [58]) can improve resistance to degradation. In particular, it is possible that given the high calculated tolerance factors, these phases are on the borderline between cubic and hexagonal perovskites. So future studies should investigate higher Fe contents to try to improve the stability.

Conclusions

In conclusion, apparent NTE at low temperatures was observed for the perovskite phases $BaFe_{0.6}Co_{0.3}Nb_{0.1}O_{3-\delta}$ (BFCN) and $BaCo_{0.7}Yb_{0.2}Bi_{0.1}O_{3-\delta}$ (BCYB) perovskites. An apparent NTE of α= -11.6x10^{-6} K^{-1} over a ΔT 140K and α= -17.3x10^{-6} K^{-1} over a ΔT 110K, respectively, were obtained. Water desorption from the structure was found to be responsible for the apparent NTE for both samples, which led to a contraction in the unit cell size and hence the observed apparent NTE. The NTE was confirmed by dilatometry and XRD analyses. Further studies of the impact of water on the stability of the BFCB and BCYB phases at SOC operating temperatures showed that a moderate humidity level of 4% had a negative effect on the long-term stability of the tested perovskite materials. Heat treatment under wet conditions led to degradation and formation of $BaCoO_{3-\delta}$. Long exposure to dry air resulted in the formation of a second cubic phase. The degradation was linked to the sintering of particles observed by SEM. This instability suggests that these materials are not suitable for application as air electrodes in SOCs. Nevertheless, their ability to incorporate water was significant and suggested work should be directed to related systems (with higher Fe contents) to deliver samples with improved moisture stability while preserving the ability to accommodate water. Such systems could then be the next generation of SOC air electrode materials suitable for use with proton-conducting electrolytes. For BCYB there was the interesting observation of two similar perovskite phases at elevated temperature.

Acknowledgements

We would like to thank EPSRC (JUICED Hub EP/R023662/1) for funding.

The authors express their thanks to CHART of the University of Birmingham for providing access to HR-TEM.

The Supporting Information and raw data are available on a website

https://doi.org/10.25500/edata.bham.00000395.

Conflict of interest

The authors declare that they have no conflict of interest.

Reference List

1. Sun C, Hui R, Roller J (2010) Cathode materials for solid oxide fuel cells: a review. J. Solid State Electrochem. 14 (7):1125-1144. doi:10.1007/s10008-009-0932-0
2. Burnwal SK, Bharadwaj S, Kistaiah P (2016) Review on MIEC Cathode Materials for Solid Oxide Fuel Cells. J. Mol. Eng. Mater. 04 (02):1630001. doi:10.1142/s2251237316300011
3. Chen Y, Zhou W, Ding D, Liu M, Ciucci F, Tade M, Shao Z (2015) Advances in Cathode Materials for Solid Oxide Fuel Cells: Complex Oxides without Alkaline Earth Metal Elements. Adv. Energy Mater. 5 (18):1500537. doi:10.1002/aenm.201500537
4. Jiang S (2008) Development of Lanthanum Strontium Manganite Perovskite Cathode Materials of Solid Oxide Fuel Cells: A Review. J. Mater. Sci. 43:6799-6833. doi:10.1007/s10853-008-2966-6
5. Shao Z, Halle SM (2004) A high-performance cathode for the next generation of solid-oxide fuel cells. Nature 431 (7005):170-173. doi:10.1038/nature02863
6. Magnone E (2010) A Systematic Literature Review on BSCF-Based Cathodes for Solid Oxide Fuel Cell Applications. J. Fuel Cell Sci. Technol. 7:064001-064012. doi:10.1115/1.4001323
7. Shen F, Lu K (2018) Comparison of Different Perovskite Cathodes in Solid Oxide Fuel Cells. Fuel Cells 18 (4):457-465. doi:10.1002/fuce.201800044
8. Tai LW, Nasrallah MM, Anderson HU, Sparlin DM, Sehlin SR (1995) Structure and electrical properties of $La_{1-x}SrxCo_{1-y}FeyO_3$. Part 2. The system $La_{1-x}SrxCo_{0.2}Fe_{0.8}O_3$. Solid State Ionics 76 (3-4):273-283. doi:10.1016/0167-2738(94)00245-N
9. Ping Jiang S (2019) Development of lanthanum strontium cobalt ferrite perovskite electrodes of solid oxide fuel cells – A review. Int. J. Hydrogen Energy 44: 7448-7493. doi:10.1016/j.ijhydene.2019.01.212
10. Kim J, Sengodan S, Kwon G, Ding D, Shin J, Liu M, Kim G (2014) Triple-Conducting Layered Perovskites as Cathode Materials for Proton-Conducting Solid Oxide Fuel Cells. ChemSusChem 7 (10):2811-2815. doi:10.1002/cssc.201402351
11. Jiang Q, Cheng J, Wang R, Fan Y, Gao J (2012) Novel triple-phase composite cathode materials for proton-conducting solid oxide fuel cells. J. Power Sources 206:47-52. doi:https://doi.org/10.1016/j.jpowsour.2012.01.084
12. Muñoz-García AB, Pavone M (2016) First-Principles Design of New Electrodes for Proton-Conducting Solid-Oxide Electrochemical Cells: A-Site Doped $Sr_2Fe_{1.5}Mo_{0.5}O_{6-\delta}$ Perovskite. Chem. Mater. 28 (2):490-500. doi:10.1021/acs.chemmater.5b03262
13. Strandbakke R, Cherepanov VA, Zuev AY, Tsvetkov DS, Argirusis C, Sourkouni G, Prünte S, Norby T (2015) Gd- and Pr-based double perovskite cobaltites as oxygen electrodes for proton ceramic fuel cells and electrolyser cells. Solid State Ionics 278:120-132. doi:https://doi.org/10.1016/j.ssi.2015.05.014
14. Choi S, Kucharczyk CJ, Liang Y, Zhang X, Takeuchi I, Ji H-I, Haile SM (2018) Exceptional power density and stability at intermediate temperatures in protonic ceramic fuel cells. Nat. Energy 3 (3):202-210. doi:10.1038/s41560-017-0085-9
15. Zohourian R, Merkle R, Raimondi G, Maier J (2018) Mixed-Conducting Perovskites as Cathode Materials for Protonic Ceramic Fuel Cells: Understanding the Trends in Proton Uptake. Adv. Funct. Mater. 28 (35):1801241. doi:doi:10.1002/adfm.201801241
16. Yasuda I, Hishinuma M (2000) Lattice Expansion of Acceptor-doped Lanthanum Chromites under High-temperature Reducing Atmospheres. Electrochem. 68 (6):526-530
17. Løken A, Ricote S, Wachowski S (2018) Thermal and Chemical Expansion in Proton Ceramic Electrolytes and Compatible Electrodes, Crystals vol 8. doi:10.3390/cryst8090365

18. Barrera GD, Bruno JAO, Barron THK, Allan NL (2005) Negative thermal expansion. J. Phys. Condens. Matter 17 (4):R217-R252. doi:10.1088/0953-8984/17/4/r03
19. Azuma M, Oka K, Nabetani K (2015) Negative thermal expansion induced by intermetallic charge transfer, Sci. Technol. Adv. Mater. 16 (3):034904. doi:10.1088/1468-6996/16/3/034904
20. Azuma M, Chen W-t, Seki H, Czapski M, Olga S, Oka K, Mizumaki M, Watanuki T, Ishimatsu N, Kawamura N, Ishiwata S, Tucker MG, Shimakawa Y, Attfield JP (2011) Colossal negative thermal expansion in $BiNiO_3$ induced by intermetallic charge transfer. Nat. Commun. 2:347. doi:10.1038/ncomms1361 https://www.nature.com/articles/ncomms1361#supplementary-information
21. Nabetani K, Muramatsu Y, Oka K, Nakano K, Hojo H, Mizumaki M, Agui A, Higo Y, Hayashi N, Takano M, Azuma M (2015) Suppression of temperature hysteresis in negative thermal expansion compound BiNi1−xFexO3 and zero-thermal expansion composite. Appl. Phys. Lett. 106 (6):061912. doi:10.1063/1.4908258
22. Pan Z, Chen J, Yu R, Patra L, Ravindran P, Sanson A, Milazzo R, Carnera A, Hu L, Wang L, Yamamoto H, Ren Y, Huang Q, Sakai Y, Nishikubo T, Ogata T, Fan Xa, Li Y, Li G, Hojo H, Azuma M, Xing X (2019) Large Negative Thermal Expansion Induced by Synergistic Effects of Ferroelectrostriction and Spin Crossover in $PbTiO_3$-Based Perovskites. Chem. Mater. 31 (4):1296-1303. doi:10.1021/acs.chemmater.8b04266
23. Chen J, Wang F, Huang Q, Hu L, Song X, Deng J, Yu R, Xing X (2013) Effectively control negative thermal expansion of single-phase ferroelectrics of PbTiO3-(Bi,La)FeO3 over a giant range. Sci. Rep. 3:2458. doi:10.1038/srep02458 https://www.nature.com/articles/srep02458#supplementary-information
24. Chen J, Fan L, Ren Y, Pan Z, Deng J, Yu R, Xing X (2013) Unusual Transformation from Strong Negative to Positive Thermal Expansion in $PbTiO_3$-$BiFeO_3$ Perovskite. Phys. Rev. Lett. 110 (11):115901. doi:10.1103/PhysRevLett.110.115901
25. Woodcock DA, Lightfoot P, Villaescusa LA, Díaz-Cabañas M-J, Camblor MA, Engberg D (1999) Negative Thermal Expansion in the Siliceous Zeolites Chabazite and ITQ-4: A Neutron Powder Diffraction Study. Chem. Mater. 11 (9):2508-2514. doi:10.1021/cm991047q
26. Lind C (2012) Two Decades of Negative Thermal Expansion Research: Where Do We Stand? Mater. 5 (6):1125-1154, doi: 10.3390/ma5061125
27. Evans JSO, Mary TA, Vogt T, Subramanian MA, Sleight AW (1996) Negative Thermal Expansion in ZrW2O8 and HfW2O8. Chem. Mater. 8 (12):2809-2823. doi:10.1021/cm9602959
28. Qi TF, Korneta OB, Parkin S, De Long LE, Schlottmann P, Cao G (2010) Negative Volume Thermal Expansion Via Orbital and Magnetic Orders in $Ca_2Ru_{1-x}Cr_xO_4$($0<x<0.13$). Phys. Rev Lett. 105 (17):177203. doi:10.1103/PhysRevLett.105.177203
29. Dove MT, Fang H (2016) Negative thermal expansion and associated anomalous physical properties: review of the lattice dynamics theoretical foundation. Rep. Prog. Phys. 79 (6):066503. doi:10.1088/0034-4885/79/6/066503
30. Ablitt C, Craddock S, Senn MS, Mostofi AA, Bristowe NC (2017) The origin of uniaxial negative thermal expansion in layered perovskites. npj Comput. Mater. 3 (1):44. doi:10.1038/s41524-017-0040-0
31. Ablitt C, Mostofi AA, Bristowe NC, Senn MS (2018) Control of Uniaxial Negative Thermal Expansion in Layered Perovskites by Tuning Layer Thickness. Front. Chem. 6 (455). doi:10.3389/fchem.2018.00455
32. Meng J, Zhang L, Yao F, Zhang X, Zhang W, Liu X, Meng J, Zhang H (2017) Theoretical Study on the Negative Thermal Expansion Perovskite $LaCu_3Fe_4O_{12}$: Pressure-Triggered Transition of Magnetism, Charge, and Spin State. Inorg. Chem. 56 (11):6371-6379. doi:10.1021/acs.inorgchem.7b00458
33. Ge X, Mao Y, Liu X, Cheng Y, Yuan B, Chao M, Liang E (2016) Negative thermal expansion and broad band photoluminescence in a novel material of $ZrScMo_2VO_{12}$. Sci. Rep. 6:24832-24832. doi:10.1038/srep24832
34. Haugsrud R (2003) On the high-temperature oxidation of nickel. Corros. Sci. 45 (1):211-235. doi:https://doi.org/10.1016/S0010-938X(02)00085-9
35. Kreuer KD (2003) Proton-Conducting Oxides. Annu. Rev. Mater. Res. 33 (1):333-359. doi:10.1146/annurev.matsci.33.022802.091825
36. Lyagaeva J, Medvedev D, Demin A, Tsiakaras P (2015) Insights on thermal and transport features of $BaCe_{0.8-x}Zr_xY_{0.2}O_{3-\delta}$ proton-conducting materials, J. Power Sources.vol 278. doi:10.1016/j.jpowsour.2014.12.024

37. Onishi T, Han D, Noda Y, Hatada N, Majima M, Uda T (2018) Evaluation of performance and durability of Ni-BZY cermet electrodes with BZY electrolyte. Solid State Ionics 317:127-135. doi:https://doi.org/10.1016/j.ssi.2018.01.015
38. Bjørheim TS, Løken A, Haugsrud R (2016) On the relationship between chemical expansion and hydration thermodynamics of proton conducting perovskites. J Mater. Chem. A 4 (16):5917-5924. doi:10.1039/C5TA10090A
39. Iwahara H, Esaka T, Uchida H, Maeda N (1981) Proton conduction in sintered oxides and its application to steam electrolysis for hydrogen production. Solid State Ionics 3-4:359-363. doi:https://doi.org/10.1016/0167-2738(81)90113-2
40. Li F, Liu X, Song W, Yuan B, Cheng Y, Yuan H, Cheng F, Chao M, liang E (2014) Phase transition, crystal water and low thermal expansion behavior of $Al_{2-2x}(ZrMg)_xW_3O_{12}\cdot n(H_2O)$. e J. Solid State Chem. 218:15-22. doi:https://doi.org/10.1016/j.jssc.2014.06.009
41. Xu X, Wang H, Fronzi M, Wang X, Bi L, Traversa E (2019) Tailoring cations in a perovskite cathode for proton-conducting solid oxide fuel cells with high performance. J. Mater. Chem. A. doi:10.1039/C9TA05300J
42. Meng Y, Gao J, Zhao Z, Amoroso J, Tong J, Brinkman KS (2019) Review: recent progress in low-temperature proton-conducting ceramics. J. Mater. Sci. 54 (13):9291-9312. doi:10.1007/s10853-019-03559-9
43. Lin Y, Zhou W, Sunarso J, Ran R, Shao Z (2012) Characterization and evaluation of $BaCo_{0.7}Fe_{0.2}Nb_{0.1}O_{3-\delta}$ as a cathode for proton-conducting solid oxide fuel cells. Int. J. Hydrogen Energy 37 (1):484-497. doi:https://doi.org/10.1016/j.ijhydene.2011.09.010
44. Cheng Y, Zhao H, Teng D, Li F, Lu X, Ding W (2008) Investigation of Ba fully occupied A-site $BaCo_{0.7}Fe_{0.3-x}Nb_xO_{3-\delta}$ perovskite stabilized by low concentration of Nb for oxygen permeation membrane. J. Membr. Sci. 322 (2):484-490. doi:https://doi.org/10.1016/j.memsci.2008.05.065
45. Zhang J, Zhao H, Li Y, Xu N, Ding W, Lu X, Li F (2010) Effects of iron content on the structural evolution, electrical properties and thermochemical stability of $BaCo_{0.9-x}Fe_xNb_{0.1}O_{3-\delta}$ ceramic membrane. Int. J. Hydrogen Energy 35 (2):814-820. doi:https://doi.org/10.1016/j.ijhydene.2009.10.101
46. Yang C, Zhao F, Chen F, Liu M (2014) Investigation of A-site deficient $Ba_{0.9}Co_{0.7}Fe_{0.2}Nb_{0.1}O_{3-\delta}$ cathode for proton conducting electrolyte based solid oxide fuel cells. Int. J. Hydrogen Energy 39 (16):8431-8436. doi:https://doi.org/10.1016/j.ijhydene.2014.03.158
47. ASTM E228−17 - Standard Test Method for Linear Thermal Expansion of Solid Materials With a Push-Rod Dilatometer.
48. Toby BH, Von Dreele RB (2013) GSAS-II: the genesis of a modern open-source all purpose crystallography software package. J. Appl. Crystallogr. 46 (2):544-549. doi:doi:10.1107/S0021889813003531
49. Yi J, Schroeder M, Weirich T, Mayer J (2010) Behavior of $Ba(Co, Fe, Nb)O_{3-\delta}$ Perovskite in CO_2-Containing Atmospheres: Degradation Mechanism and Materials Design. Chem. Mater. 22 (23):6246-6253. doi:10.1021/cm101665r
50. Sahini MG, Tolchard JR, Wiik K, Grande T (2015) High temperature X-ray diffraction and thermo-gravimetrical analysis of the cubic perovskite $Ba_{0.5}Sr_{0.5}Co_{0.8}Fe_{0.2}O_{3-\delta}$ under different atmospheres. Dalton Trans. 44 (23):10875-10881. doi:10.1039/C4DT03963G
51. Papargyriou D, Irvine J (2015) Nickel nanocatalyst exsolution from (La,Sr) $(Cr,M,Ni)O_3$ (MMn,Fe) perovskites for the fuel oxidation layer of Oxygen Transport Membranes. Solid State Ionics 288. doi:10.1016/j.ssi.2015.11.007
52. Waidha AI, Ni L, Ali J, Lepple M, Donzelli M, Dasgupta S, Wollstadt S, Alff L, Kramm UI, Clemens O (2020) Synthesis of bifunctional $BaFe_{1-x}Co_xO_{3-y-\delta}(OH)_y$ catalysts for the oxygen reduction reaction and oxygen evolution reaction. J. Mater. Chem. A 8 (2):616-625. doi:10.1039/C9TA10222A
53. Taguchi H, Komatsu T, Chiba R, Nozawa K, Orui H, Arai H (2011) Characterization of $LaNi_xCo_yFe_{1-x-y}O_3$ as a cathode material for solid oxide fuel cells. Solid State Ionics 182 (1):127-132. doi:https://doi.org/10.1016/j.ssi.2010.11.015
54. Radaelli PG, Cheong SW (2002) Structural phenomena associated with the spin-state transition in $LaCoO_3$. Phys. Rev. B 66 (9):094408. doi:10.1103/PhysRevB.66.094408

55. Yi J, Feng S, Zuo Y, Liu W, Chen C (2005) Oxygen Permeability and Stability of $Sr_{0.95}Co_{0.8}Fe_{0.2}O_{3-\delta}$ in a CO_2- and H_2O-Containing Atmosphere. Chem. Mater. 17 (23):5856-5861. doi:10.1021/cm051636y
56. Zhu J, Andres CM, Xu J, Ramamoorthy A, Tsotsis T, Kotov NA (2012) Pseudonegative Thermal Expansion and the State of Water in Graphene Oxide Layered Assemblies. ACS Nano 6 (9):8357-8365. doi:10.1021/nn3031244
57. Andres CM, Zhu J, Shyu T, Flynn C, Kotov NA (2014) Shape-Morphing Nanocomposite Origami. Langmuir 30 (19):5378-5385. doi:10.1021/la404955s
58. Geng Z, Ding W, Wang H, Wu C, Shen P, Meng X, Gai Y, Ji F (2012) Influence of barium dissolution on microstructure and oxygen permeation performance of $Ba_{1.0}Co_{0.7}Fe_{0.2}Nb_{0.1}O_{3-\delta}$ membrane in aqueous medium. J. Membr. Sci. 403–404:140–145. doi:10.1016/j.memsci.2012.02.030